

Design Of PV Powered Electric Vehicle Charging Station Using ANFIS Controller for Energy Management

K. SURYANARAYANAMURTHY¹, PROF. M. GOPICHAND NAIK², SREYAS VELLANKI³

^{1,2}Dept. of Electrical, AU College of Engineering, Visakhapatnam. India

³Sri Chaitanya Junior College, Visakhapatnam. India

Abstract— The focus of this paper is on effectively managing power distribution among various sources. With the escalating concerns of global warming and climate change due to the surging demand for modern transportation systems, there is a burgeoning advocacy for Electric Vehicles (EVs) to address these issues. However, relying solely on fossil fuel-based infrastructure for charging EVs is neither economically viable nor efficient. This underscores the substantial potential of utilizing renewable energy sources for EV charging stations. To meet this requirement, the integration of a solar-powered EV charging station with a Battery Energy Storage System (BESS) is imperative. To ensure consistent power supply without straining the grid, it is advisable to incorporate additional grid support. Furthermore, an LLC was specifically designed at the grid to minimize the current distortion introduced into the utility grid. To achieve optimal power management across the solar panels, BESS, grid, and EVs, a well-structured charging station employing an Adaptive Neuro-Fuzzy Inference System (ANFIS) with voltage-controlled Maximum Power Point Tracking (MPPT), PID control, and Neural Network techniques has been developed and assessed using MATLAB/Simulink.

Index Terms- Electric Vehicles, Battery energy storage system, Adaptive Neuro-Fuzzy Inference System, MPPT, PID controller, Neural Network, PV.

I. INTRODUCTION

As the demand for modern transportation systems continues to grow, global warming and climate change are becoming more severe due to the pollutants emitted by internal combustion engine vehicles (ICEs), which significantly contribute to air pollution and greenhouse gas emissions. Electric vehicles (EVs) offer a promising alternative to traditional gasoline-powered cars. EVs are gaining popularity due to their more efficient electric motors compared to ICEs, leading to energy savings, reduced noise, and lower pollution levels. They also help reduce reliance on oil

for transportation, provided that the electricity used to charge them comes from non-oil sources. However, as the number of EVs on the road increases, the task of charging these vehicles using electricity from the grid becomes more challenging. The integration of a large number of EVs can strain grid operations and control. Furthermore, using traditional energy sources to charge EVs does not offer significant environmental benefits.

Therefore, there is a need for efficient EV charging infrastructure that relies on renewable energy sources, complemented by a Battery Energy Storage System (BESS) as a buffer between the EV Charging Station (EVCS) and the utility. Although BESS can help alleviate some of the strain on the utility grid, the anticipated large number of EVCSs in the future continues to present a significant challenge. The charging methods of EVs are categorized into different power levels as per SAE J1772 standard, which is summarized in Table 1. The most common household slow charging method is AC Level 1, where the EV can be plugged into any convenient power outlet. AC Level 2 is a semi-fast charging method that requires a 240V/400V outlet, while AC Level 3 is a three-phase fast charging method that operates at 208/415V. The DC fast charging method used in charging stations is intended for public and commercial usage. Reference (8) explores the integration of Battery Energy Storage Systems (BESS) with solar photovoltaic (PV) technology at EV

Level Types	Voltage	Power Level	Charging Time
AC Level 1	120 Vac (US)	1.4 kW (12 A)	14 - 17 h
	230 Vac (EU)		
AC Level 2	240 Vac	4 kW (17 A)	4 - 6 h

2	(US)	A)	
	400 Vac (EU)		
AC Level 3	230 Vac/415 Vac	>20 kW	0.4 - 1 h
DC Level 1	200 - 450 Vdc	36 kW (80 A)	0.4 - 1 h
DC Level 2	200 - 450 Vdc	90 kW (200 A)	10 -20 mins
DC Level 3	200 - 600 Vdc	240 kW (400 A)	<10 mins

Table 1 Standard EV charging levels (SAE J1772)

charging stations. Reference (9) covers the implementation and management of power flow for renewable energy systems, including both wind energy conversion systems (WECS) and PV arrays, in the context of EV charging. Reference (11) examines the use of solar power and battery storage for EV charging within a workspace, while reference (12) addresses the application of maximum power point tracking for standalone PV arrays using an adaptive neuro-fuzzy inference system.

In the proposed work, a anfis based approach is utilized for managing power in a solar-powered EV charging station with an integrated BESS connected to the AC grid. An Adaptive Neuro-Fuzzy Inference System (ANFIS) with voltage control is employed to optimize the electricity harvested from the solar panels under varying irradiance and temperature conditions.

The ANFIS (Adaptive Neuro-Fuzzy Inference System) manages the power output from the AC grid by considering both solar power production and the state of charge (SOC) of the Battery Energy Storage System (BESS). When solar irradiance is high, the PV system primarily supplies power for EV charging, with any surplus energy being fed into the AC grid to recharge the BESS. During nighttime or when solar power is insufficient, the BESS supplies energy for EV charging. If both solar and BESS power are unavailable, the AC grid can be utilized to maintain a continuous power supply. This proposed system has been simulated using MATLAB/Simulink

II. EV CHARGING STATION MODEL

A suggested solar-powered charging station with energy storage in the form of a battery and AC grid is depicted schematically in Fig.1. A 450V DC bus with one EV battery is considered at a time for proposed work. All the component’s technical specifications are shown in Table I.

A. PV array with a Boost converter

In MATLAB/Simulink, a 35kW PV panel with a 35.6V at maximum power point (MPP) voltage is investigated for the charging station design. To acquire the needed DC bus voltage of 450V, a boost converter is employed to step up the PV array voltage and an ANFIS voltage controller with Proportional-Integral (PI) controller is utilized to get the most power out of the PV array.

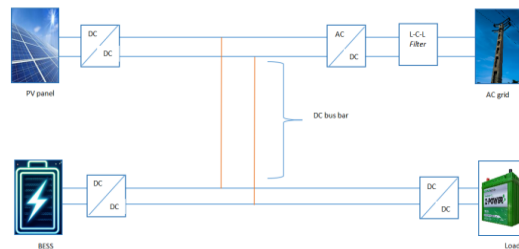


Fig. 1. Representation of EV charging station

TABLE II. Charging Station Data

Module Data	
Number of cells	60
Open circuit voltage	37.3 V
Short-circuit current	8.66 A
Voltage at MPPT	31.3 V
Current at MPPT	8.03 A
Array Data	
Parallel cells	12
Series connected modules per string	12
BESS Data	
Nominal voltage	320 V
Rated capacity	100 kWh
Battery type	Lithium-ion
EV Battery Data	
Nominal voltage	320 V
Rated capacity	36kWh
The initial state of charge	9 %

Battery type	Lithium-ion
--------------	-------------

(BESS) Battery Energy Storage System with Bidirectional Boost DC-DC converter

Solar energy is harvested and stored in a Battery Energy Storage System (BESS), which is then used to charge electric vehicles during nighttime. The BESS’s charging and discharging processes are managed by a bidirectional boost DC-DC converter. The charging station employs a 320V, 100kWh BESS, which is expected to discharge to a minimum of 20% State of Charge (SOC).

Grid with Inverter

The 230V, 50Hz AC grid is being considered to meet the additional power needs of the charging station. In MATLAB/Simulink, a 230V AC source represents the grid. This AC grid is linked to a 450V DC bus via an inverter. A neural network Simulink model is developed to generate pulses for the inverter switches, using the PV array output power and the BESS’s %SOC as input data for the neural network.

EV Battery

A 320V, 36kwh battery is considered for the charging station. The EV battery is charged from a 400V DC bus using a PI controller for the DC-DC boost converter. For simulation purposes, the incoming EV battery is expected to have a minimum of 9% State of Charge (SOC). The energy required to charge the EV battery can be calculated using the nominal voltage, the remaining %SOC, and the battery’s Ampere-hour (Ah) rating.

III. CONTROL METHODOLOGY

1. Adaptive Neuro-Fuzzy Inference System (ANFIS)

An Adaptive Neuro-Fuzzy Inference System (ANFIS) is a network that emulates the behavior of both neural networks and fuzzy inference systems. Unlike traditional neural networks, ANFIS does not use synaptic weights but instead features non-adaptive and adaptive nodes. This structure allows it to be transformed into a typical feedforward neural network, hence the term “adaptive network.”

The ANFIS structure is similar to that of the adaptive Takagi-Sugeno fuzzy controller’s network emulator. It operates in the same manner as a fuzzy inference system (FIS). Techniques such as back-propagation gradient descent and least-squares are used to adjust the input and output parameters of the ANFIS network based on the given input/output data set. These parameters are categorized as linear and nonlinear. The ANFIS network is divided into two main sections: the antecedent and the consequent parts, which are connected by a rule-based fuzzy inference system. Figure 1 illustrates the five-layer structure of ANFIS. Layer 1: This layer contains adaptive nodes, where the nonlinear parameters of the ANFIS network are located. The function of each node in this layer is expressed by Eq. (2).

$$L_{1,i} = \mu A_i(e) \text{ for } i=1, 2, \dots, j \text{ -----(1)}$$

$$L_{1,i} = \mu B_i(\Delta e) \text{ for } i=1, 2, \dots, j \text{ -----(2)}$$

where (e) and (Δ e) are the inputs to node (i) in layer 1. The membership functions for each node are denoted as (A_i) and (B_i). Typically, the membership function for each node is assigned based on the input variables, which are distributed using a Gaussian membership function. The Gaussian membership function is formulated as follows, resulting in Eq. (3).

$$f(x; \sigma, c) = e^{-\frac{(x-c)^2}{2\sigma^2}} \text{ -----(3)}$$

where (σ) and (c) represent the width and center of the Gaussian membership function, respectively. These nonlinear parameters are adjusted during the learning process.

Layer 2: This layer consists of fixed nodes, denoted by the symbol “Π”. The output of each node in this layer is the product of the signals from the nodes in Layer 1. The node function is expressed by Eq. (4).

$$L_{2,k} = \mu A_i(e) \mu B_i(\Delta e) \text{ for } i=1, 2, \dots, j^2 \text{ -----(4)}$$

The output of each layer 2 node determines the rule base’s firing strength

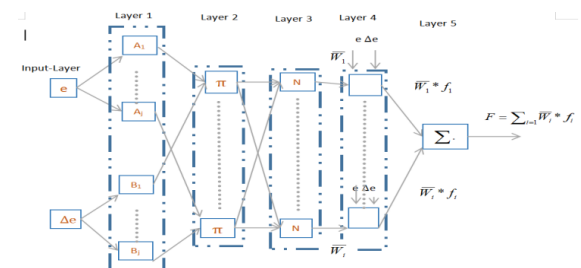


Fig. 2. Five-layer adaptive neuro-fuzzy inference system structure

Layer 3: This layer consists of fixed nodes, denoted by the letter “N.” The output of each node in this layer is determined by dividing the value of the node by the sum of the values of all nodes. The node function is expressed by Eq. (5).

$$L_{3,i} = \bar{W}_i = \frac{W_i}{\sum_{i=1}^{j^2} W_i} \text{-----(5)}$$

Layer 4: This node is flexible. Eq. (6) expresses the functionality of this node as,

$$L_{4,i} = \bar{W}_i f_i = \bar{W}_i (p_i + q_i \Delta e + r_i) \text{---(6)}$$

Where (W_i) represents the normalized firing strength in Layer 3, and (p_i, q_i, r_i) are the linear parameters of the ANFIS network, also referred to as the network’s consequent parameters. These parameters are adjusted using the least-squares method during the learning phase.

Layer 5: This layer is denoted by the symbol “Σ” and consists of fixed nodes known as the output layer. The output from this layer is calculated using the weighted average technique, as given by Eq. (7).

$$L_{5,i} = \sum_{i=1}^{j^2} \bar{W}_i f_i = \frac{\sum_{i=1}^{j^2} W_i f_i}{\sum_{i=1}^{j^2} W_i} \text{-----(7)}$$

A hybrid technique is employed to update the nonlinear and linear parameters of Layer 2 and Layer 4. This hybrid algorithm for ANFIS parameters combines the steepest descent and least-squares methods.

The hybrid method utilizes two types of propagation: forward and backward. During forward propagation, the output of the nodes is passed up to Layer 4, and the linear parameters are adjusted using the least-squares approach. In backward propagation, the error signals are propagated backward, and the nonlinear parameters are modified using gradient descent. This hybrid approach converges much faster than conventional back-propagation algorithms because the dimensions of the search space are significantly reduced during training.

2. Maximum power point tracking with an adaptive neuro-fuzzy inference system-PI controller.

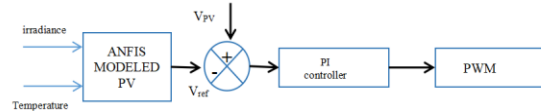


Fig 3. ANFIS voltage-controlled MPPT

In this MPPT structure, ANFIS is utilized to create a model of a solar PV system that closely replicates the original. ANFIS is trained with two inputs—irradiance and temperature—and one output—voltage—under varying irradiance and temperature conditions. The voltage reference is obtained from the ANFIS system’s output and is compared to the actual PV voltage to generate an error voltage. This error voltage is processed by a proportional-integral (PI) controller, which produces a duty cycle for the PWM generator. The PWM generator then generates pulses for a DC-DC boost converter to extract the maximum power from the solar PV array.

3. ANFIS - based AC grid

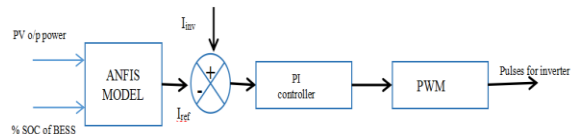


Fig 4. Block diagram of ANFIS model

The data of PV array output power, varying with irradiance and the SOC of the BESS, is used to develop a anfis model in MATLAB/Simulink. The current reference is obtained from this anfis Simulink model and is compared to the AC grid, inverter current to generate a current error. This error is processed by a proportional-integral (PI) controller, which then produces a duty cycle for the inverter.

4. L-C-L filter

The LCL-filter is a third order filter having attenuation of 60db/decade for frequencies above full resonant frequency, hence lower switching frequency for the converter switches could be utilized . Decoupling between the filter and the grid connected inverter having grid side impedance is better for this situation and lower current ripple over the grid inductor might be attained.

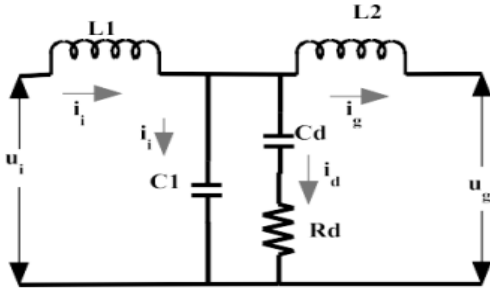


Fig. 5. Single Phase Equivalent Circuit of an LCL Filter with Passive Damping

The LCL filter will be vulnerable to oscillations too and it will magnify frequencies around its cut-off frequency. Therefore the filter is added with damping to reduce the effect of resonance. Therefore LCL-filter fits to our application. In the interim, the aggregate inductance of the received LCL filter is much more diminutive as contrasted with the L filter. Commonly, the expense is lessened. Besides, enhanced dynamic execution, harmonic attenuation and decreased volume might be accomplished with the utilization of LCL filter. The conduction and switching losses that are caused by the filter are calculated and are optimized considering the level of reduction of harmonics.

Table 3: Filter design specifications

Parameter	Value
Grid Voltage	230 V
Output Power of the Inverter	35KVA
DC-Link voltage	450 V
Grid frequency	50 Hz
Switching frequency	10kHz
Power factor	1

During design of L-C-L filter it is important to take care of some necessary factors. This factor includes inverter output ripple current, inverter to grid inductor ratios and filter capacitance maximum power variations. Typically current ripple is usually limited to 10%-25%, inverter to grid ratio is between 0-1, the capacitor value is limited to less than 5% of the decrease of the rated power and ripple attenuation must be less than 20%. The inverter to grid side inductance ratio is derived based on the equation 8.

This factor is obtained from the ratio between the filter impedance and the difference between resonant frequency and switching frequency. Thus, this ratio is the key factor for the desired ripple attenuation of the filter which is given as the ratio of

$$\frac{i_g(h)}{i(h_{sw})} = \frac{1}{\{1 + r * [1 - (c_b * L * \omega_{sw}^2) * x]\}} \quad \text{-----}$$

(8)

Whereas, r , C_b and x are the relation factor between inductances, base capacitance and the filter capacitance factor.

Therefore based on the important factors in estimating L-C-L filter, this paper uses output ripple current of 10% of the rated output current.

$$\Delta I_L = 10\% * \frac{\sqrt{2} * P_N}{V_{phase_grid}} \quad \text{-----}(9)$$

The value of the ripple output current is used in estimating the value of the inverter side inductance L_i

$$L_i = \frac{V_{DC}}{16 * f_s * \Delta I_L} \quad \text{-----}(10)$$

Inverter inductance L_i and grid inductance L_g are related with r in equation 10. If 5% is taken as attenuation factor of the filter, then the approximated value of $r = 0.6$.

$$L_g = r * L_i \quad \text{-----}(11)$$

The filter capacitance C_f of the L-C-L filter in this thesis is limited to 5% of the rated output power. Usually is taken as the fraction of the base capacitance, C_b

$$C_f = 5\% C_b = 0.05 * \frac{P_N}{(\omega_{grid} * U^2)_{Phase_grid}} \quad \text{-----}(12)$$

The passive damping resistor, R_d , is obtained at the resonance frequency, f_0 of the L-C-L filter. The values of damping resistance and resonance frequency are given in the equations 13 and 14 respectively.

$$R_d = \frac{1}{3 * \omega_o * C_f} \quad \text{-----}(13)$$

$$f_o = \frac{1}{2\pi} * \sqrt{\frac{L_i + L_g}{L_i * L_g * C_f}} \quad \text{-----}(14)$$

Resonance frequency is then calculated by using the filters components in equation 14.

Then the damping resistance R_d is found to be 0.755Ω . Filter components are summarized in

Table 4: L-C-L filter components

Components	Value
Inverter side inductor L_i	$145\mu\text{H}$
Filter capacitor, C_f	$105\mu\text{F}$
Grid side inductor, L_g	$87\mu\text{H}$
Damping resistance, R_d	0.755Ω
Resonance frequency, f_0	20.7kHz

IV. OPERATION OF EV OFF-BOARD CHARGER

A. Operational modes

Mode 1: The electric vehicle (EV) battery is charged solely by the photovoltaic (PV) array. In this mode, the temperature is kept constant while the irradiance of the PV panel is adjusted. The maximum power from the PV array is managed using an Adaptive Neuro-Fuzzy Inference System (ANFIS) with a voltage-controlled approach is shown in fig 5.

Mode 2: Both the EV battery and the Battery Energy Storage System (BESS) are charged exclusively with solar power when the BESS is connected to the DC bus. The PV panel operates at its Maximum Power Point Tracking (MPPT) using ANFIS is shown in fig 6.

Mode 3: The EV battery is charged using a combination of solar power and BESS, with varying irradiance levels. ANFIS is used to maximize the power extraction from the PV array.

Mode 4: At night, when the PV array's irradiance is zero, the EV battery is charged using power from the AC grid and BESS. ANFIS controls the power flow from the AC grid.

Simulation Results

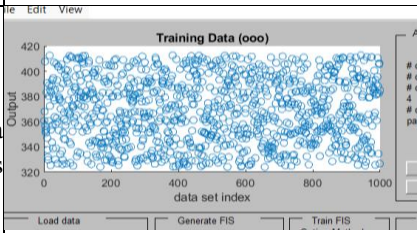
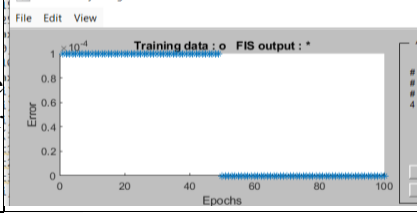
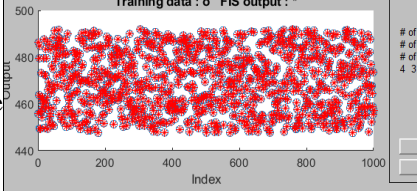
The constructed Simulink model is evaluated for varying sun irradiation levels and temperature levels.

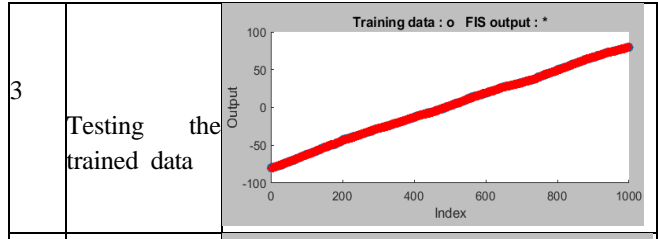
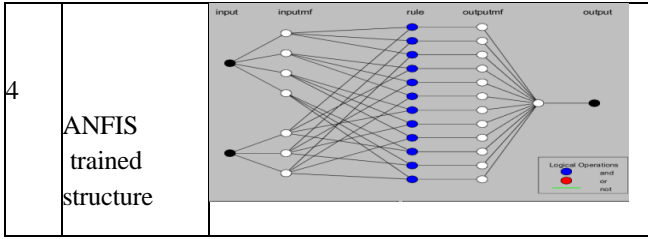
The Simulink model of a ANFIS based PV-powered EV charging station is displayed in Figure 5.2

A. ANFIS controller training with a PV array model

The data collected from the PV array serves as the foundation for training the ANFIS voltage controller. This process involves measuring the voltage at the maximum power point as it varies with temperature and irradiance. Once this data is imported, the grid partition method of subtractive clustering is employed to define the membership functions for the inputs. Subsequently, the ANFIS controller undergoes training through a hybrid learning approach, with a total of 100 iterations being evaluated. Following this training phase, the controller is tested with a set of test data to ensure its accuracy and reliability. Upon successful testing, the ANFIS controller is converted into a reference PV model. Table 5 provides a comprehensive illustration of the training process and performance of the ANFIS controller in MATLAB, showcasing its capacity to optimize the voltage control in the PV array system efficiently.

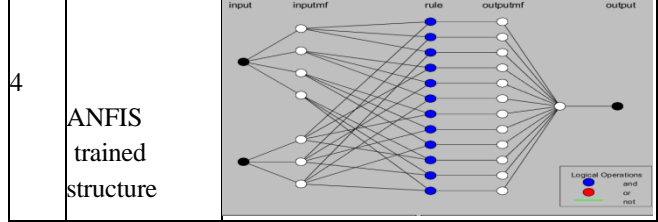
TABLE 5. TRAINING OF ANFIS CONTROLLER

S.No	Phases in training ANFIS	Representation of training phases in MATLAB
1	Output data of Anfis modeled PV	
2	Training the error plot for 100 epochs	
3	Testing the trained data	



B. ANFIS controller training for generating reference current(i_{ref})

The data from the PV array and BESS is used to train the ANFIS controller. The power at the maximum power point is measured as a function varying irradiance and also SOC of BESS. After importing this data, the grid partition method of subtractive clustering is used to define the membership function for the inputs. The ANFIS controller is trained using a hybrid learning approach, with 100 iterations being evaluated. The ANFIS controller will then be tested with test data. After it has been properly tested, the ANFIS controller is converted into a reference model for generating reference current(i_{ref}) then compared with inverted current and processed to the pi controller thereby it is used for generating pulses for the inverter. Table 6 illustrates the ANFIS controller's MATLAB training.



1st mode :Temperature is maintained constant at 250 C and Irradiance of PV array is varied in steps, PV power is 35kW at maximum irradiance of 1000 W/m2 . PV voltage is constant and PV power varies with the variation of irradiance which ensures the maximum power extraction from the PV array as shown in Fig. 6

TABLE 6. Training Of ANFIS Controller For Grid

S.No	Phases in training ANFIS	Representation of training phases in MATLAB
1	Output data of Anfis model	
2	Training the error plot for 100 epochs	

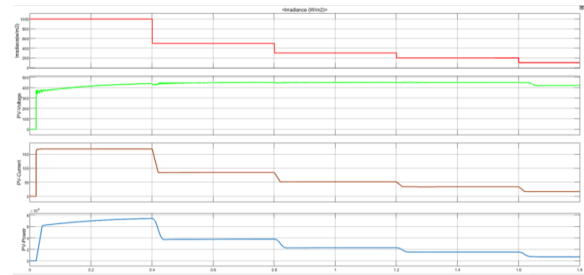


Fig. 6. PV Voltage, current, and power with a variation of irradiance

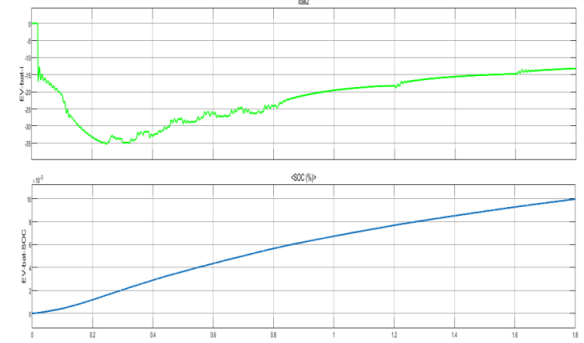


Fig. 7. EV battery charging current and % SOC

C. 2nd mode: Both the BESS and EV battery is charged as shown in Fig. 8. With the extraction of maximum power available from PV array at different irradiance and temperature which is shown in Fig. 9.

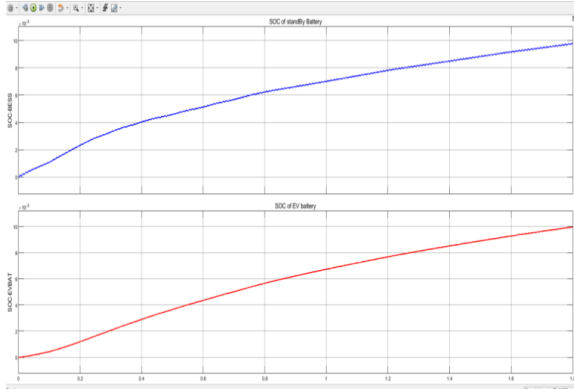


Fig. 8. % SOC of BESS and EV battery

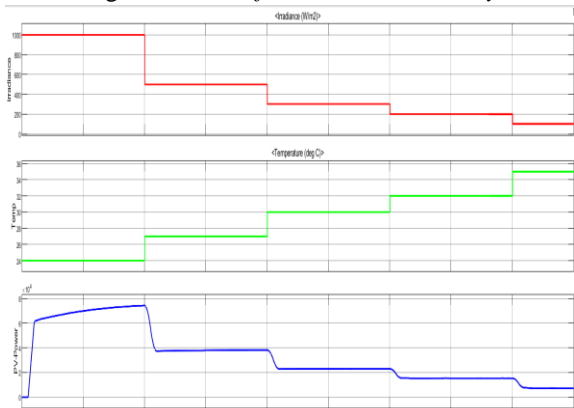


Fig. 9. DC bus voltage, PV output power, Irradiance, and temperature of PV array

3rd mode: The DC bus connects the PV array, BESS, and EV battery, DC bus voltage of 450V is maintained and power is transferred from the PV array to the DC bus with the variation of irradiance and temperature of the PV array as shown in Fig. 10 EV battery is charged by taking power from DC bus and BESS, Fig. 11 Shows that energy is transferred from BESS which is represented by decreasing of %SOC of BESS and charging of EV battery which is represented by increasing of %SOC of EV battery

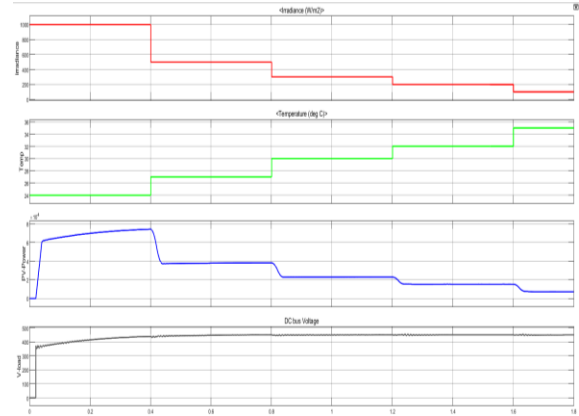


Fig. 10. %SOC of BESS and EV battery

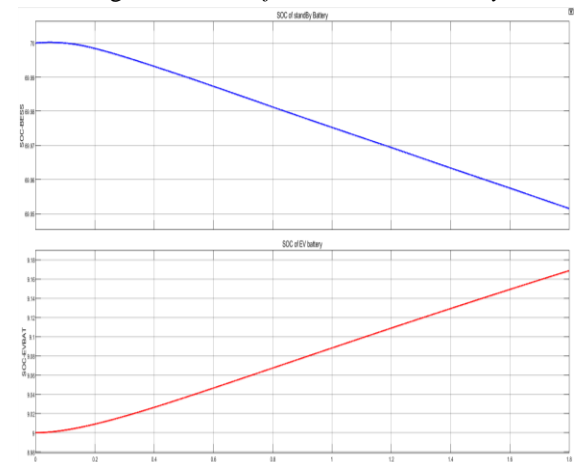


Fig. 11. Grid supplied power when PV output power is zero

4th mode: During night power supplied by PV array is zero, at simulation time of 0.1sec ANFIS network start controlling the power flow from the grid as shown in Fig. 12. AC grid is connected to the DC bus through the inverter. Fig. 13. shows the grid voltage and current through the inverter when the grid is supplying power to the DC bus. Charging of EV battery from DC bus is shown in Fig. 14

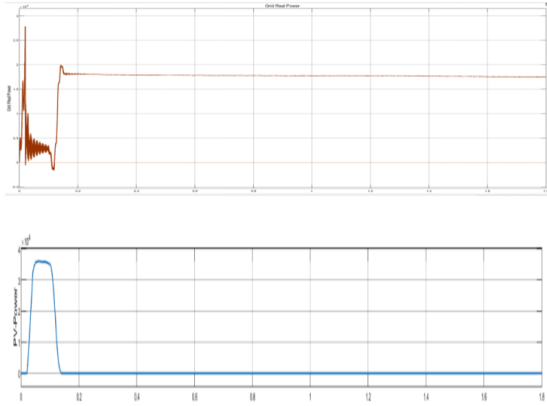


Fig. 12. Grid supplied power when PV output power is zero

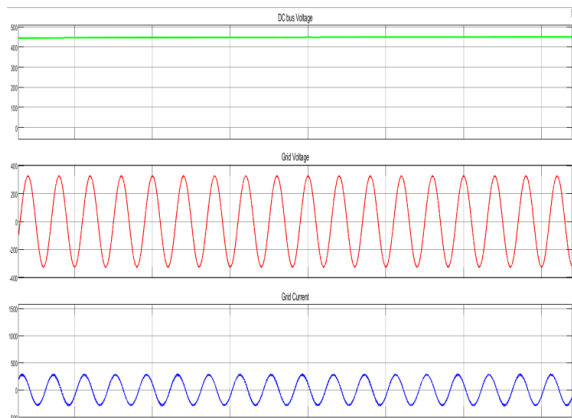


Fig. 13. DC bus voltage, Grid voltage, and grid current

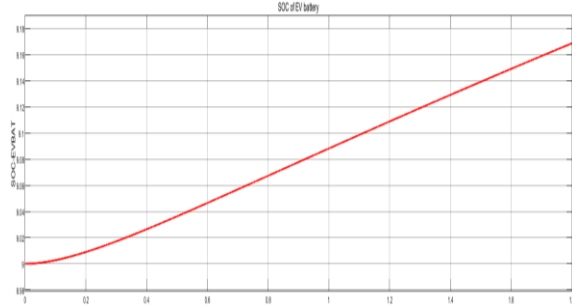


Fig. 14. Charging of EV battery represented by increasing %SOC

MODE 5: At a simulation time of 0.1 seconds, the ANFIS begins controlling the AC grid power. Between 0.1 seconds and 0.4 seconds, the grid's real power shows a negative value, indicating that power is being supplied to the AC grid from the DC bus, as illustrated in Fig. 14. The Battery Energy Storage System (BESS) provides power to the DC bus, while the EV battery charges from this DC bus, as depicted in Fig. 15.

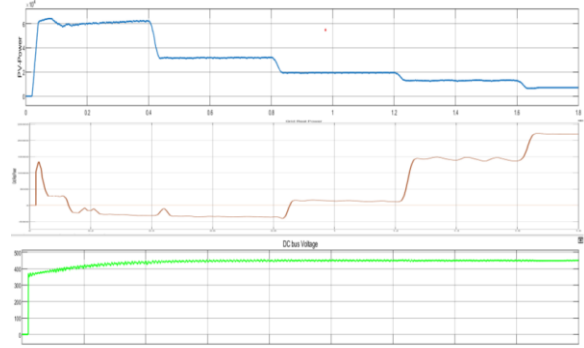


Fig. 14. DC bus voltage, Power supplied by PV array, and Grid real power

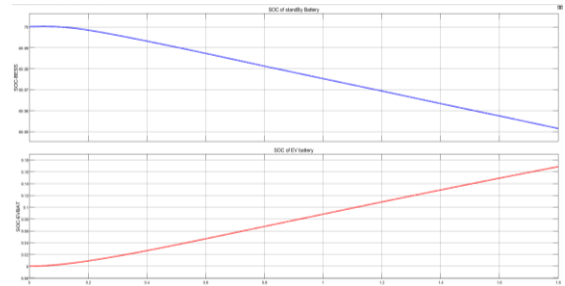


Fig. 15. BESS supplying energy to DC bus and Charging of EV battery

CONCLUSION

As the number of electric vehicles are increasing on the road, EV charging has become a significant concern. A promising solution involves a charging station powered by a photovoltaic (PV) array combined with a battery energy storage system (BESS), enhanced by grid support. To meet the charging needs of all connected electric vehicles, ANFIS voltage control, a PI controller, and a anfis are utilized. By maintaining a steady DC bus voltage, the desired power can be achieved, ensuring the station's bus voltage remains constant. The proposed station's power management is discussed and validated using MATLAB/Simulink in five distinct modes. Further exploration of the proposed model for a larger number of electric vehicles can be implemented, with a significant power rating and capacity for power supply, making it suitable for EV charging stations at workplaces or parking lots.

REFERENCES

- [1] García-Vidal, J., & Pinto, M. (2020). "Neural Networks for Energy Forecasting in Solar PV Systems." *Renewable Energy*.
- [2] Khan, M. J., et al. (2021). "Smart Electric Vehicle Charging Station Management Using Machine Learning." *IEEE Access*.
- [3] Moussa, A. H., & Abdallah, S. (2022). "A Review of PV-powered Electric Vehicle Charging Stations." *Energy Reports*.
- [4] Zhou, H., et al. (2019). "Optimization of Electric Vehicle Charging Using Neural Networks and Big Data." *IEEE Transactions on Smart Grid*.
- [5] Samuel Vasconcelos Araújo, Alfred Engler, Fernando Luiz and Marcelo Antunes. LCL Filter design for grid-connected NPC inverters in offshore wind turbines. The 7th International Conference on Power Electronics, ICPE'07, pp 1133-1138, EXCO, Daegu, Korea October 2007.
- [6] Pérez, A., & Mendoza, J. (2023). "Integrating Machine Learning with Renewable Energy for Electric Vehicle Charging." *IEEE International Conference on Smart Energy Systems*.
- [7] Zhe Yu; Shiyao Chen; "an intelligent energy management system for large-scale charging of electric vehicles," in 2019 *CSEE Journal of Power and Energy Systems*
- [8] M. Fatnani, D. Naware, and A. Mitra, "Design of Solar PV Based EV Charging Station with Optimized Battery Energy Storage System," 2020 IEEE First International Conference on Smart Technologies for Power, Energy and Control (STPEC), 2020
- [9] A. Verma and B. Singh, "An Implementation of Renewable Energy Based Grid-Interactive Charging Station," in 2019 IEEE Transportation Electrification Conference and Expo (ITEC), 2019,
- [10] I. Colak, R. Bayindir, A. Aksoy, E. Hossain, and S. Sayilgan, "Designing a competitive electric vehicle charging station with solar PV and storage," 2015 IEEE International Telecommunications Energy Conference (INTELEC), 2015,
- [11] K. S. Vikas, B. Raviteja Reddy, S. G. Abijith and M. R. Sindhu, "Controller for Charging Electric Vehicles at Workplaces using Solar Energy," 2019 International Conference on Communication and Signal Processing (ICCSP), 2019, pp.
- [12] N. Priyadarshi, V. K. Ramachandaramurthy, S. Padmanaban, F. Azam, A. K. Sharma, and J. P. Kesari, "An ANFIS Artificial Technique Based Maximum Power Tracker for Standalone Photovoltaic Power Generation," 2018 2nd IEEE International Conference on Power Electronics, Intelligent Control, and Energy Systems (ICPEICES), 2018, pp.
- [13] K. Premkumar, B. Manikandan, "Adaptive Neuro Fuzzy Inference System based speed controller for brushless DC motor," 2014.
- [14] K. Premkumar, B. Manikandan, "Adaptive Neuro-Fuzzy Inference System based speed controller for brushless DC motor," 2014. [15] K. Premkumar, B. Manikandan, "Stability and performance analysis of ANFIS tuned PID based speed controller for brushless DC motor," 2018.
- [15] IEEE Recommended Practice for Utility Interface of Photovoltaic (PV) Systems, IEEE Std 929-2000, January, 2000.
- [16] Svein Erik Evju. Fundamentals of Grid Connected Photovoltaic Power Electronic Converter Design. Specialization project, Department of Electric Engineering, Norwegian University of Science and Technology, December 2006.
- [17] J. Bauer. Single Phase Voltage Source Inverter Photovoltaic Application. Acta Polytechnica, Vol. 50, No. 4, pp 7-11, 2010.
- [18] Ofualagba Gods will, Onyan Aaron Okiemute and Igbino Charles. Design of a Photovoltaic Grid-Connected DC-AC Inverter. International Journal of Emerging trends in Engineering and Development, ISSN: 2249 – 6149. Vol.4, No.2, pp 1-16, May, 2012.
- [19] Bijoyprakash Majhi. Analysis of Single-Phase SPWM Inverter. Master's thesis, Department of Electrical Engineering National Institute of Technology, Rourkela May 2012